International Journal of Biological Macromolecules 164 (2020) 2795–2803

Contents lists available at ScienceDirect

International Journal of Biological Macromolecules

journal homepage: http://www.elsevier.com/locate/ijbiomac

Highly regio- and enantio-selective hydrolysis of two racemic epoxides by *Gm*EH3, a novel epoxide hydrolase from *Glycine max*

Chen Zhang [a,1], Chuang Li [b,1], Xiu-xiu Zhu [a], You-yi Liu [c], Jun Zhao [d,*], Min-chen Wu [c,*]

[a] School of Pharmaceutical Science, Jiangnan University, Wuxi 214122, PR China
[b] College of Biological and Chemical Engineering, Auhui Polytechnic University, Wuhu 241000, PR China
[c] Wuxi School of Medicine, Jiangnan University, Wuxi 214122, PR China
[d] The Affiliated Wuxi Matemity and Child Health Care Hospital of Nanjing Medical University, Wuxi 214002, PR China

ARTICLE INFO

Article history:
Received 18 June 2020
Received in revised form 28 July 2020
Accepted 2 August 2020
Available online 04 August 2020

Keywords:
Epoxide hydrolase
Glycine max
Regio- and enantio-selective hydrolysis
m-Chlorostyrene oxide
Phenyl glycidyl ether
Molecular docking simulation

ABSTRACT

A novel epoxide hydrolase from *Glycine max*, designated *Gm*EH3, was excavated based on the computer-aided analysis. Then, *gmeh3*, a *Gm*EH3-encoding gene, was cloned and successfully expressed in *E. coli* Rosetta(DE3). Among the ten investigated *rac*-epoxides, *Gm*EH3 possessed the highest and best complementary regioselectivities (regioselectivity coefficients, $\alpha_S = 93.7\%$ and $\beta_R = 97.2\%$) in the asymmetric hydrolysis of *rac*-*m*-chlorostyrene oxide (**5a**), and the highest enantioselectivity (enantiomeric ratio, $E = 55.6$) towards *rac*-phenyl glycidyl ether (**7a**). The catalytic efficiency ($k^S_{cat}/K^S_m = 2.50$ mM^{-1} s^{-1}) of purified *Gm*EH3 for (*S*)-**5a** was slightly higher than that ($k^R_{cat}/K^R_m = 1.52$ mM^{-1} s^{-1}) for (*R*)-**5a**, whereas the k_{cat}/K_m (5.16 mM^{-1} s^{-1}) for (*S*)-**7a** was much higher than that (0.09 mM^{-1} s^{-1}) for (*R*)-**7a**. Using 200 mg/mL wet cells of *E. coli*/*gmeh3* as the biocatalyst, the scale-up enantioconvergent hydrolysis of 150 mM *rac*-**5a** at 25 °C for 1.5 h afforded (*R*)-**5b** with 90.2% ee_p and 95.4% yield$_p$, while the kinetic resolution of 500 mM *rac*-**7a** for 2.5 h retained (*R*)-**7a** with over 99% ee_s and 43.2% yield$_s$. Furthermore, the sources of high regiocomplementarity of *Gm*EH3 for (*S*)- and (*R*)-**5a** as well as high enantioselectivity towards *rac*-**7a** were analyzed via molecular docking (MD) simulation.

1. Introduction

Epoxide hydrolases (EHs, EC 3.3.2.-), existing diffusely in almost all living organisms, can catalyze the hydrolysis of racemic (*rac*-) epoxides to their corresponding 1,2-diols [1]. Most of known EHs belong to an α/β-hydrolase fold superfamily, and are divided into two major regions in spatial structure: an α/β domain, i.e., a β-sheet surrounded by a cluster of α-helices, and a cap domain, which is inserted by a cap-loop varied in peptide length as well as residue composition [2]. The substrate-binding pocket (SBP) is situated between the two above-mentioned domains, harboring a catalytic triad (Asp-His-Asp/Glu) and two specific Tyr residues serving as proton donors [3]. Generally, the ring-opening hydrolysis of epoxides by α/β-hydrolase fold EHs proceeds in the following steps (Fig. 1). The substrate is first activated via the formation of hydrogen bonds with two proton donors. Secondly, two carbon atoms (C_α and C_β) in the oxirane ring of (*S*)- or (*R*)-epoxide are regioselectively attacked by a nucleophilic side-chain oxygen of Asp residue in EH's catalytic triad, forming an EH-hydroxyalkyl intermediate. Finally, a water molecule activated by general-base His and charge-relay Asp/Glu interacts with the intermediate, generating a 1,2-diol [4]. Based on the stereochemical outcomes of specific EH-epoxide pairs, the asymmetric hydrolysis of *rac*-epoxides was generally classified into two major pathways: the kinetic resolution and enantioconvergent hydrolysis [5]. EHs applied in the kinetic resolution of *rac*-epoxides must have high enantioselectivity (*E* value), thus, retaining enantiomeric epoxides with over 99% enantiomeric excess (ee_s) and up to 50% maximum yield$_s$, and in the enantioconvergent hydrolysis both high regiocomplementarity and low *E* value, producing chiral 1,2-diols with high enantiopurity (ee_p) and up to 100% theoretical yield$_p$ [6].

Enantiopure epoxides and 1,2-diols are versatile and highly value-added building blocks for synthesis of pharmaceutical, fine chemical and agrochemical products [7]. For examples, (*S*)-**5a** is used for the synthesis of BMS-536924, an IGF-1R kinase inhibitor for regulation of in vivo antitumor activity [8,9], while (*S*)-**7a** for (*S*)-Levobunolol, a β-adrenergic blocking agent applied in the treatment of glaucoma [10,11]. With the sustainable development of global industrialization, the biocatalysis by whole cells or enzymes has been regarded as a fungible method for chemocatalysis that requires expensive chiral ligands, environment-unfriendly catalysts and harsh reaction conditions, exampled by Jacobsen epoxidation and Sharpless dihydroxylation [12]. The regio- and enantio-selective hydrolysis of *rac*-epoxides by EHs, an economical and sustainable way with satisfactory enantiopurity and yield of the target products, is considered to have great application prospects in producing enantiopure epoxides and 1,2-diols [13]. To date,

* Corresponding authors.
E-mail addresses: chalange@163.com (J. Zhao), biowmc@126.com (M. Wu).
[1]Chen Zhang and Chuang Li, the two first authors, contributed equally to this work.

https://doi.org/10.1016/j.ijbiomac.2020.08.011
0141-8130/

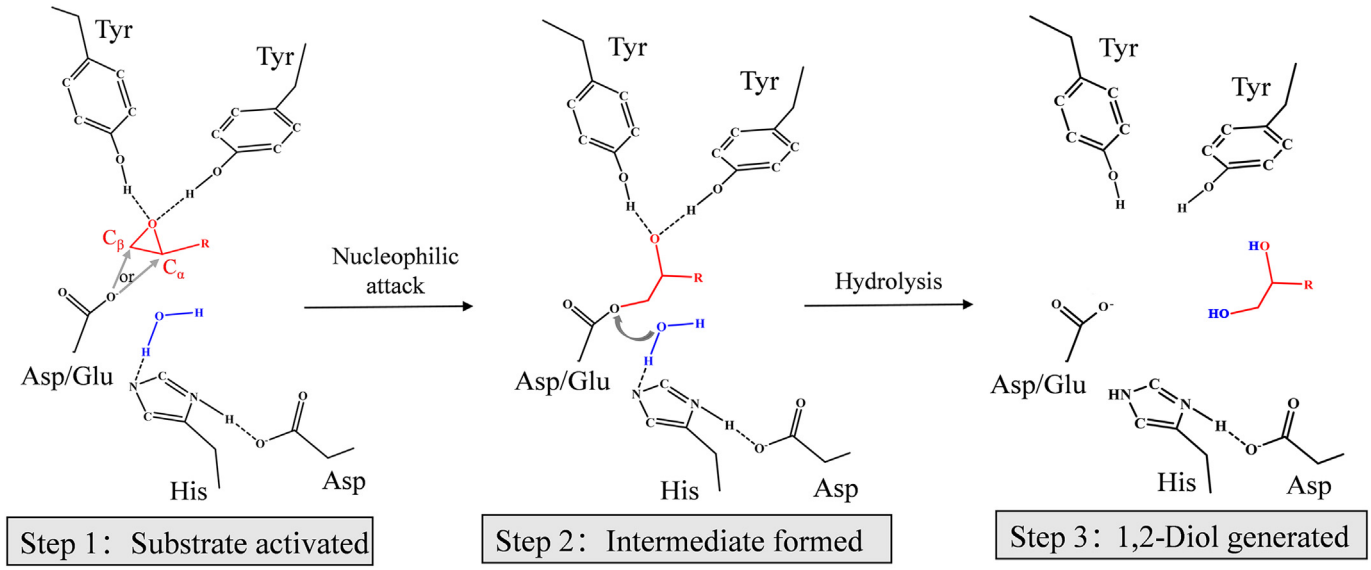

Fig. 1. The hydrolytic mechanism of α/β-hydrolase fold EHs.

numerous EHs have been heterogeneously expressed, characterized, and modified. However, to our knowledge, a certain EH is not likely to catalyze a variety of *rac*-epoxides optimally. Reportedly, a plant-derived EH, *Sl*EH1, can mediate the kinetic resolution reactions of epoxy styrene derivatives effectively, but displayed very low enantioselectivities ($E = 1.0$–2.3) towards glycidyl ether and aliphatic chain epoxide derivatives [14]. For another example, an *Aspergillus usamii* EH (*Au*EH2), only its catalytic properties in stereoselective ring-opening of *rac*-**1a** was investigated, however, its moderate *E* value and low regiocomplementarity resulted in merely 38.0% $yield_s$ of retained (*S*)-**1a** (99.2% ee_s) and very low ee_p of (*R*)-1-phenyl-1,2-ethanediol, that is (*R*)-**1b** [15]. Therefore, to provide more options for efficiently producing chiral epoxides and 1,2-diols with high enantiopurities (ee_s and ee_p) and yields ($yield_s$ and $yield_p$) from diverse *rac*-epoxides, it is necessary to excavate novel EHs with excellent catalytic properties and expected stereochemical outcomes, and/or to reshape some local structures of existing EHs by protein engineering [16].

Selecting the sequence of a characterized *Phaseolus vulgaris* EH (*Pv*EH3, GenBank no. ATG22745) [17] as the template, a hypothetical EH from *G. max* (XP_006604802), renamed *Gm*EH3 in this work, was explored based on the homologous sequence search and multiple sequence alignment. Then, the gene coding for *Gm*EH3, *gmeh3*, was amplified from *G. max* total RNA by RT-PCR, and successfully expressed in *E. coli* Rosetta(DE3). The substrate spectrum assay of *Gm*EH3 towards ten *rac*-epoxides (**1a**–**10a**) was carried out using whole cells of *E. coli*/*gmeh3* (Fig. 2). The intracellularly expressed *Gm*EH3 was purified to homogeneity, whose kinetic parameters, such as K_m and V_{max}, for (*S*)- and (*R*)-**5a** (or **7a**) were assayed. Additionally, the scale-up enantioconvergent hydrolysis of *rac*-**5a** and kinetic resolution of *rac*-**7a** at high concentrations were conducted, respectively, using whole cells of *E. coli*/*gmeh3*. Moreover, the molecular mechanisms of *Gm*EH3 with high and complementary regioselectivities for (*S*)- and (*R*)-**5a** as well as high enantioselectivity towards *rac*-**7a** were elucidated via analyzing and comparing the parameters of simulatedly docked EH-epoxide complexes.

2. Materials and methods

2.1. Strains, plasmids, and chemicals

E. coli JM109 and plasmid pUCm-T (Sangon, Shanghai, China) were applied to gene cloning, while *E. coli* Rosetta(DE3) and a cold-shock pCold II (TaKaRa, Dalian, China) to the expression of *gmeh3*. All enzymes and kits for *G. max* total RNA extraction and *gmeh3* manipulation were purchased from Sangon or TaKaRa. *Rac*-**1a**, **6a**–**10a**, and (*S*)- and (*R*)-**5a** (and **7a**) were from Energy (Shanghai, China), while *rac*-**2a**–**5a** were chemically synthesized in our lab (Table S1). Other chemicals were of analytical grade, and commercially available from the local companies (Wuxi, China).

2.2. Exploration in GenBank database and analysis of EH sequences

Using a characterized EH, *Pv*EH3, as the template, several hypothetical plant EH sequences with unknown functions were searched at NCBI website (https://www.ncbi.nlm.nih.gov/) by a BLAST server. Among them, a hypothetical *G. max* EH (h*Gm*EH, XP_006604802), which shared the highest primary structure identity, was selected. The multiple sequence alignment of h*Gm*EH with six characterized plant-derived EHs was conducted using the ESPript 3.0 server (http://espript.ibcp.fr/). Based on the analysis of their conserved motifs, h*Gm*EH was identified as the research object. Additionally, the phylogenetic tree of various representative EHs was built using the Observed Divergency method in the DNAMAN 6.0 software (https://www.lynnon.com/).

2.3. Enzyme activity and protein assays

The hydrolytic conditions of *rac*-**1a** for *Gm*EH3 activity assay were set as follows: 950 μL *E. coli*/*gmeh3* cell suspension or purified *Gm*EH3 solution, suitably diluted with 100 mM Na_2HPO_4-NaH_2PO_4 buffer (pH 7.0), was well mixed with 50 μL 200 mM *rac*-**1a** (at the final concentration of 10 mM), incubated at 25 °C for 10 min, and terminated by addition of 4 mL methanol. Then, the hydrolytic sample was analyzed by high-performance liquid chromatography (HPLC), using an e2695 apparatus (Waters, Milford, MA) equipped with an XBridge BEH C18 column. The mobile phase of methanol/H_2O (7:3, v/v) was applied at 0.8 mL/min, and real-time monitored using a Waters 2489 UV–Vis detector. One unit (U) of EH activity was defined as the amount of whole wet cells of *E. coli*/*gmeh3* or purified *Gm*EH3 hydrolyzing 1 μmol *rac*-**1a** per minute under the above conditions. Analogously, the hydrolytic reactions of 10 mM *rac*-**2a**–**10a** for the assay of *Gm*EH3 activities were carried out, respectively, by substituting *rac*-**1a** with them. The hydrolytic samples were analyzed by HPLC and gas chromatography (GC) using a GC-2010 apparatus (Shimadzu, Tokyo, Japan), equipped with various chiral chromatography columns at the operating conditions

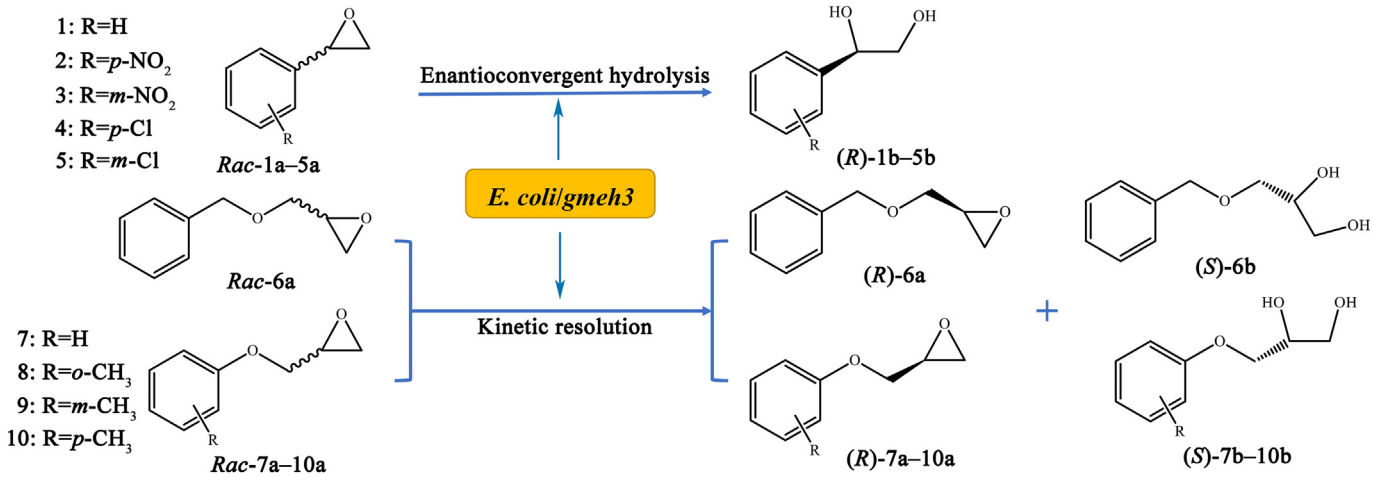

Fig. 2. Stereoselective hydrolysis of ten *rac*-epoxides (*rac*-**1a**–**10a**) using whole cells of *E. coli*/*gmeh3*.

corresponding to these columns, which are entirely dependent on the physicochemical properties of retained epoxides and/or generated 1,2-diols (Table S2).

The expression level of *Gm*EH3 and its purification grade were visually assayed by sodium dodecyl sulfate-polyacrylamide gel electrophoresis (SDS-PAGE) on a 12% agarose gel. Its apparent molecular weight (MW) was estimated using the Quantity One software (https://www.bio-rad.com/) by comparison with those of the standard proteins. The protein concentration was determined using a BCA-200 protein assay kit (Pierce, Rockford, IL), using bovine serum albumin as the standard.

2.4. Cloning and expression of a gene encoding GmEH3

Several mature soybean (*G. max*) seeds from the local supermarket (Wuxi, China) were soaked, and incubated at 27 °C for three days. Then, the sprouts were harvested, and washed with phosphate buffer. The total RNA was extracted using the UNIQ-10 column Trizol total RNA isolation kit, from which *gmeh3* was amplified using the PrimeScript RT-PCR kit. Firstly, a pair of PCR primers, *gmeh3*-F (5′-CATATGGAGGGAATAGA GCACAGGACAG-3′) and *gmeh3*-R (5′-CTCG AGTCAAAACTTGTTGATGAAATCGTGT-3′) flanked by *Nde* I and *Xho* I sites, were designed according to the 5′- and 3′-end nucleotide sequences of the h*Gm*EH-encoding mRNA (XM_006604739) and synthesized by Sangon. Secondly, the first-strand cDNAs were reversely transcribed from the total RNA using an Oligo dT-Adaptor primer provided by RT-PCR kit according to its protocol. Then, using the transcribed cDNAs as templates, *gmeh3* was amplified with the above primers, *gmeh3*-F and -R, as following conditions: an initial denaturation at 94 °C for 3 min, 30 cycles of at 94 °C for 30 s, 55 °C for 30 s and 72 °C for 60 s, and an extra elongation at 72 °C for 10 min. Finally, the amplified target PCR product, *gmeh3*, was directly ligated with a linearized pUCm-T and transformed into *E. coli* JM109, followed by DNA sequencing.

The correct *gmeh3* was excised from a recombinant plasmid, pUCm-T-*gmeh3*, by *Nde* I and *Xho* I, and then inserted into pCold II digested with the same restriction endonucleases. The resulting recombinant plasmid, pCold II-*gmeh3*, was transformed into *E. coli* Rosetta(DE3), constructing an *E. coli* transformant, *E. coli*/*gmeh3*. Comparatively, *E. coli* Rosetta(DE3) transformed with pCold II, *E. coli*/pCold II, was used as the negative control. The expression of *gmeh3* was carried out as previously described [18], except for induction by 0.05 mM IPTG at 15 °C for 14 h. The induced *E. coli*/*gmeh3* cells were harvested by centrifugation, and resuspended in 100 mM phosphate buffer (pH 7.0) to 200 mg/mL wet cells, unless stated otherwise, used as the whole-cell biocatalyst.

2.5. Investigation of enantio- and regio-selectivities of GmEH3

The hydrolytic reactions of *rac*-epoxides, in ten aliquots of 3 mL 100 mM phosphate buffer (pH 7.0) systems consisting of 20 mM *rac*-**1a**-**10a**, respectively, and a certain amount of *E. coli*/*gmeh3* wet cells, were conducted at 25 °C. During the hydrolytic process of each *rac*-epoxide, aliquots of 50 μL samples were drawn periodically, extracted with 950 μL ethyl acetate, and analyzed by chiral HPLC or GC (Table S2). The conversion ratio (c) of each *rac*-epoxide was defined as the percentage of its hydrolyzed amount to initial amount, while the yield_s of an enantiomeric epoxide such as (R)-**7a** (or yield_p of a chiral 1,2-diol such as (R)-**5b**) was referred as the percentage of its retained (or its generated) amount to initial one of *rac*-epoxide. The absolute configurations of enantiomers of *rac*-**1a**–**10a** and *rac*-**1b**–**10b** were confirmed by comparing their peaking sequences with the corresponding ones reported previously [7,15,16]. The ee_s of epoxide enantiomers and ee_p of 1,2-diols were calculated according to the equations: $ee_s = [(R_s - S_s) / (R_s + S_s)] \times 100\%$ and $ee_p = [(R_p - S_p) / (R_p + S_p)] \times 100\%$, in which R_s and S_s were the instantaneous concentrations of (R)- and (S)-epoxides, while R_p and S_p the concentrations of (R)- and (S)-1,2-diols.

The E value was applied to evaluate the degree of enantiopreferential hydrolysis of one enantiomer over its antipode. Based on the c and ee_s values determined above, the E value of *Gm*EH3 was calculated: $E = \ln[(1-c)\times(1-ee_s)] / \ln[(1-c)\times(1+ee_s)]$ [7]. When the substrates were a pair of enantiomers of a given *rac*-epoxide, the E value, having enantiopreference for (S)-form, also can be derived via calculating the ratio of catalytic efficiency, that is, $(k^S_{cat}/K^S_m)/(k^R_{cat}/K^R_m)$. Additionally, the regioselectivity coefficients, α_S (or $\beta_S = 1 - \alpha_S$) and β_R (or $\alpha_R = 1 - \beta_R$), of an EH for (S)- and (R)-enantiomers were used to estimate the probabilities attacking on the C_α (a more hindered carbon atom in the oxirane ring) of (S)-enantiomer and the C_β (a less hindered terminal carbon) of (R)-form, respectively [14]. The α_S and β_R values of *Gm*EH3 for (S)- and (R)-**5a** (or **7a**) can be directly obtained according to the concentration ratios of produced (R)- and (S)-**5b** (or **7b**), respectively. Besides, based on the c, ee_s and ee_p values those were measured at different time points, the α_S and β_R values of *Gm*EH3 for the other eight pairs of (S)- and (R)-enantiomers of epoxides (*rac*-**1a**–**4a**, **6a**, **8a**–**10a**) were derived from linear regression: $ee_p = (\alpha_S + \beta_R - 1) + [(\beta_R - \alpha_S)\times ee_s \times (1-c)]/c$ [14].

2.6. Purification of the intracellularly expressed GmEH3

The IPTG-induced and harvested *E. coli*/*gmeh3* cells, intracellularly expressing *Gm*EH3 with a 6 × His tag at its N-terminus, were suspended

in buffer A (20 mM Tris–HCl, 500 mM NaCl and 30 mM imidazole, pH 7.5) to 100 mg/mL wet cells. After disrupting the cells by ultrasonic and removing cell debris, the resulting supernatant was loaded onto a nickel-nitrilotriacetic acid (Ni-NTA) affinity column (Tiandz, Beijing, China) preequilibrated with buffer A, and followed by elution at 0.4 mL/min with buffer B as the same as buffer A, except for 300 mM imidazole. Aliquots of 1 mL eluents only containing the target EH assayed by SDS-PAGE were pooled, dialyzed against 20 mM phosphate buffer (pH 7.0), and concentrated using a 10 kDa cut-off ultrafilter membrane (Millipore, Billerica, MA).

2.7. Assay of the kinetic parameters of purified GmEH3 towards enantiomeric **5a** or **7a**

The initial hydrolytic rates (μmol/min/mg protein) of (*S*)- and (*R*)-**5a** (or **7a**) catalyzed by purified *Gm*EH3 were determined under the EH activity assay conditions, except for the concentrations of (*S*)- and (*R*)-**5a** (or **7a**) ranging from 0.5 to 20 mM. Both the K_m and V_{max} values of *Gm*EH3 were calculated by non-linear regression analysis using an Origin 9.0 software (http://www.orignlab.com/). The turnover rates (k_{cat}) of *Gm*EH3 for (*S*)- and (*R*)-**5a** (or **7a**) was deduced from its apparent MW and V_{max}, while its catalytic efficiency (k_{cat}/K_m) was defined as the ratio of k_{cat} to K_m. All kinetic parameters from three independent replicates were expressed as the mean ± standard deviation (SD).

2.8. Scale-up enantioconvergent hydrolysis of rac-**5a** by E. coli/gmeh3

The regioselective hydrolytic reactions, in four aliquots of 2 mL 100 mM phosphate buffer (pH 7.0) systems containing 200 mg/mL wet cells of *E. coli/gmeh3* and *rac*-**5a** at concentrations ranging from 50 to 200 mM, were carried out, respectively, at 25 °C within 8.0 h. Using the *c* and ee_p values as the criteria, the maximum allowable concentration (MAC) of *rac*-**5a** was first confirmed. Subsequently, the scale-up enantioconvergent hydrolysis of *rac*-**5a** at MAC was carried out in the 50 mL phosphate buffer system. During the hydrolytic process, aliquots of 50 μL reaction samples were drawn periodically, extracted with 950 μL ethyl acetate, and then analyzed by chiral HPLC with a Chiralcel OD-H column (Daicel, Osaka, Japan) until *rac*-**5a** was almost completely hydrolyzed ($c > 99\%$). In addition, the space-time $yield_p$ (STY_p, g/L/h) of (*R*)-**5b**, which was defined as the amount of (*R*)-**5b** produced from *rac*-**5a** per unit volume and time, was calculated to evaluate its production efficiency.

2.9. Scale-up kinetic resolution of rac-**7a** by E. coli/gmeh3

The enantioselective hydrolytic reactions, in six aliquots of 2 mL 100 mM phosphate buffer (pH 7.0) systems consisting of 200 mg/mL wet cells and *rac*-**7a** at elevated concentrations from 100 to 600 mM, were conducted, respectively, at 25 °C within 8.0 h, and analyzed by chiral HPLC with the Chiralcel OD-H column (Table S2). Using the ee_s and $yield_s$ of (*R*)-**7a** as the criteria, the MAC of *rac*-**7a** was confirmed. The gram-scale kinetic resolution of *rac*-**7a** at MAC in the 30 mL phosphate buffer system was conducted until the ee_s of (*R*)-**7a** reached over 99%. The STY_s (g/L/h) of (*R*)-**7a** was defined as the amount of (*R*)-**7a** retained from *rac*-**7a** per unit volume and time.

2.10. Homology modeling of GmEH3 and enantiomeric **5a** or **7a**

Using a known crystal structure of a *Vigna radiata* EH (*Vr*EH1, PDB: 5XMD) at 2.00 Å resolution as template, which shares 72.3% primary structure similarity with *Gm*EH3, the three-dimensional (3-D) structure of *Gm*EH3 was homologically modeled using MODELLER 9.21 program (https://salilab.org/modeller/), and then subjected to the molecular mechanics optimization using the CHARMM27 force field in the GROMACS 4.5 package (https://www.gromacs.org/). One 3-D conformation with the best geometry quality was selected from all the output ones, and further validated using the SAVES program (http://services.mbi.ucla.edu/SAVES/). Synchronously, the 3-D structures of four enantiomeric substrates, (*S*)- and (*R*)-**5a** (and **7a**), were constructed and disposed in minimized energy using the MM2 force field in the ChemBioOffice 2010 package (https://www.cambridgesoft.com/).

2.11. Molecular docking simulation of GmEH3 with enantiomeric **5a** or **7a**

The mutual action between the modeled 3-D structures of *Gm*EH3 and (*S*)- or (*R*)-**5a** (or **7a**) was predicted by MD simulation using the AutoDock vina program (https://autodock.scripps.edu/), and optimized by the GROMACS 4.5 package to locate the most appropriate binding sites and steric orientation, that is, a binding state having the lowest binding free energy ($\Delta G_{binding}$) [15]. The $\Delta G_{binding}$ value of each docked complex was calculated by using the molecular mechanics Poisson-Boltzmann surface area (MM-PBSA) method [16]. Based on the 3-D conformations of simulatedly docked EH-epoxide complexes, such as *Gm*EH3-(*S*)-**5a** and -(*S*)-**7a**, the through-space distances (d_α and d_β) and the hydrogen bond lengths (l_1 and l_2) were identified using a PyMol software (http://pymol.org/). The d_α or d_β was defined as the distance between the nucleophilic side-chain oxygen of Asp^{101} residue in *Gm*EH3 and C_α or C_β in the oxirane ring of (*S*)- or (*R*)-**5a** (or **7a**), as well as the l_1 or l_2 was the hydrogen bond length from the hydroxyl group of Tyr^{152} or Tyr^{234} residue (proton donor) to the oxygen atom in an oxirane ring.

3. Results and discussion

3.1. Excavation of a novel EH based on the computer-aided analysis

One h*Gm*EH, which shared the highest sequence identity of 81.3% with a characterized *Pv*EH3 [17], was selected. Then, its multiple sequence alignment with six known plant EHs (sharing over 55% identity with h*Gm*EH) was carried out (Fig. 3a). The alignment result indicated that h*Gm*EH contained the three typical conserved motifs existing in all α/β-hydrolase fold EHs: HGXP, GXSmXS/T and SmXNuXSmSm, in which X, Sm and Nu were any, small and nucleophilic residues, respectively [14,18]. It was confirmed that HGXP motif forms an oxyanion hole to stabilize the negative charge of a nucleophilic side-chain oxygen of Asp in EH's catalytic triad during the hydrolysis [19]. The catalytic triad of h*Gm*EH was confirmed as Asp^{120}-His^{316}-Asp^{281}. In addition, its two proton donors were also conserved as Tyr^{169} and Tyr^{251}. It was verified that two specific Tyr residues play important roles in substrate binding and ring-opening via forming hydrogen bonds with the oxygen atom in oxirane ring [4,20]. Owing to the above analytic results, it was speculated that h*Gm*EH may have catalytic activity towards epoxides. Thus, h*Gm*EH was renamed as *Gm*EH3, and identified as the research object for the cloning and heterologous expression of a gene coding for *Gm*EH3, as well as the investigation of its catalytic performances. Furthermore, the phylogenetic tree analysis on the sequences of h*Gm*EH and 14 representative EHs revealed that h*Gm*EH (or *Gm*EH3) was closely related to plant EHs, but relatively distant from those of other species (Fig. 3b).

3.2. Cloning and intracellular expression of gmeh3

An about 1.0-kb nucleotide sequence of *gmeh3* was amplified from *G. max* total RNA, ligated with pUCm-T, and transformed into *E. coli* JM109. DNA sequencing result verified that *gmeh3* (GenBank no. MN833949) was exactly 963 bp in length (excluding *Nde* I and *Xho* I restriction sites), encoding *Gm*EH3 (GenBank no. QJC19071) with 320 amino acid (aa) residues. The catalytic triad of *Gm*EH3, deduced from the sequences of cloned *gmeh3*, was confirmed as Asp^{101}-His^{299}-Asp^{264}, while its proton donors as Tyr^{152} and Tyr^{234}. Its sequence identities with h*Gm*EH and six known plant EHs were listed as follows: h*Gm*EH (XP_006604802, 93.4%), *Pv*EH3 (AKJ75509, 85.3%) [17],

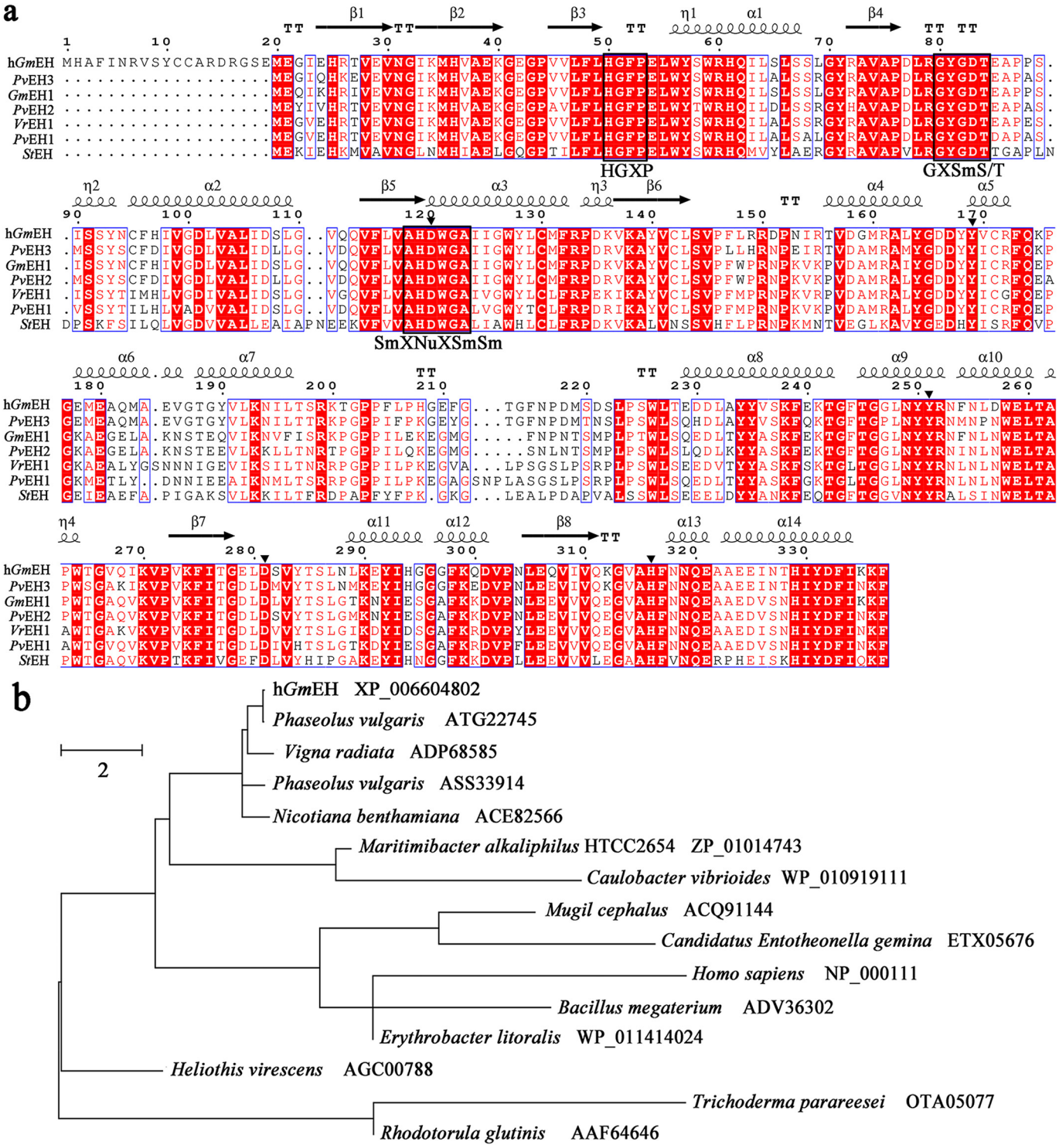

Fig. 3. (a) The multiple alignment of h*Gm*EH with six characterized plant EHs. The three conserved motifs: HGXP, GXSmXS/T and SmXNuXSmSm, were shown in black boxes. The catalytic triad (Asp^{120}-His^{316}-Asp^{281}) and proton donors (Tyr^{169} and Tyr^{251}) were marked by inverted triangles. (b) The phylogenetic tree of EHs amino acid sequences. The original species and Genbank numbers of EHs were exhibited.

*Gm*EH1 (CAA55294, 79.1%) [21], *Pv*EH2 (ASS33914, 74.7%) [18], *Vr*EH1 (ADP68585, 72.3%) [22], *Pv*EH1 (ATG22745, 70.3%) [23] and *St*EH (AAA81891, 56.6%) [24]. The cloning of *gmeh3* and its further expression not only enriched the information on EH genes and EHs, but also afforded a possible method for production of enantiopure epoxides or 1,2-diols via the kinetic resolution or enantioconvergent hydrolysis of *rac*-epoxides.

After induction at 15 °C for 14 h, the EH activity of *E. coli*/*gmeh3* towards *rac*-**1a** was measured to be 28.2 U/g wet cell (wc), whereas no EH activity was detected in *E. coli*/pCold II cells under the same expression conditions. SDS-PAGE analysis displayed that the apparent MW of expressed *Gm*EH3, which was fused with an extra 35-aa oligopeptide harboring a 6 × His tag at its N-terminus, was about 37.4 kDa (Fig. 4, lane 3), was very close to its theoretical one (37,446 Da) predicted by

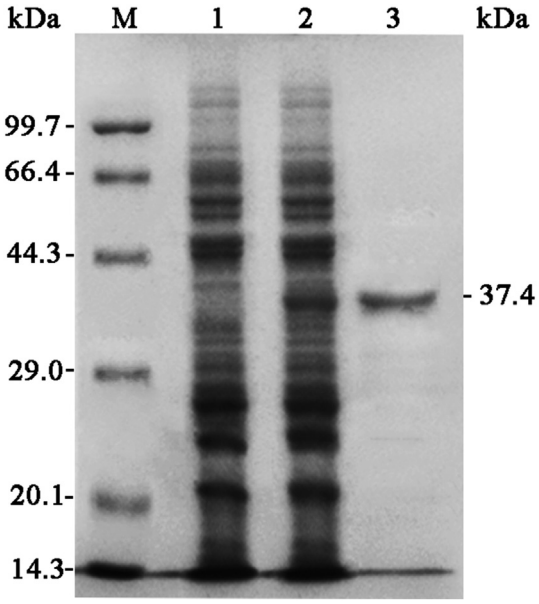

Fig. 4. SDS-PAGE of the expressed and purified *Gm*EH3. Lane M, standard protein marker; Lanes 1 and 2, the supernatant of *E. coli*/pCold II and *E. coli/gmeh3*, respectively. Line 3, the purified *Gm*EH3.

DNAMAN 6.0 software. No target protein band was found in *E. coli*/pCold II (Fig. 4, lanes 1 and 2). To develop the industrial applications of *E. coli/gmeh3* cells (or purified *Gm*EH3) in the kinetic resolution and/or enantioconvergent hydrolysis of *rac*-epoxides, its EH activities towards *rac*-**2a**–**10a** were also assayed (Table 1). The EH activities of *E. coli/gmeh3* towards ten *rac*-epoxides were determined as 2.6 to 35.1 U/g wc, which were generally higher than the corresponding data of *E. coli/vreh3* and */pveh2* [7,18]. For examples, the EH activities of the latter two *E. coli* transformants towards *rac*-**1a** were only 5.2 and 8.0 U/g wc, respectively, which were much lower than that (28.2 U/g wc) of *E. coli/gmeh3*.

3.3. Regioselectivities of GmEH3 for (S)- and (R)-1a–5a

The regioselectivity coefficients (α_S and β_R), quantitatively representing its regioselectivities for (*S*)- and (*R*)-enantiomers, used to elucidate the ee_p of an enantiomeric 1,2-diol produced from enantioconvergent hydrolysis of *rac*-epoxide (Fig. S1) [14]. In this work, the substrate spectrum assay exhibited that hydrolytic reactions of 20 mM *rac*-**1a**–**5a** using 20 mg/mL wet cells produced (*R*)-**1b**–**5b** with high ee_p from 72.1 to 90.1% and $yield_p$ from 71.2 to 94.5% (Table 1). The source of higher enantioconvergence of *Gm*EH3 towards *rac*-**1a**–**5a** was that it had high and complementary regioselectivities (α_S = 85.2–93.7% and β_R = 87.4–97.5%), together with low enantioselectivities (E = 1.3–8.2). To a given EH, its regioselectivity coefficient is tightly dependent on the catalyzed *rac*-epoxide, that is, which carbon atom (C_α or C_β) may mainly be subjected to nucleophilic attack by Asp in EH's catalytic triad [14]. Among the tested *rac*-**1a**–**5a**, *Gm*EH3 possessed the highest α_S of 93.7% for (*S*)-**5a** and β_R of 97.2% for (*R*)-**5a**, along with a lower *E* value of 1.6 and a higher EH activity of 22.4 U/g wc, thereby efficiently producing (*R*)-**5b** with 90.1% ee_p and 94.5% $yield_p$. There were many wild-type (WT) EHs with high *E* values towards *rac*-**1a**–**5a**. For example, *St*EH had *E* values of 30 and 70 towards *rac*-**1a** and **4a** [21,22]. However, few WT EHs possessed superior regiocomplementarities for (*S*)- and (*R*)-epoxides, especially for (*S*)- and (*R*)-**5a**, As shown in Table S3, the enantioconvergent hydrolysis of *rac*-**5a** by *E. coli/vreh3* or purified *St*EH produced (*R*)-**5b** with 60.9 or 88% ee_p [7,25], all lower than that (90.1% ee_p) using *E. coli/gmeh3*. Fallaciously, the ee_p of (*R*)-**5b** produced by *E. coli/gmeh3* was still slightly lower than that (96.1% ee_p) of *E. coli/pveh1*^{Y3Z2}, an *E. coli* transformant expressing a multiple-site *Pv*EH1 mutant [26].

3.4. Enantioselectivities of GmEH3 towards rac-6a–10a

The EH enantiomeric ratio (*E*), quantitatively describing its enantioselectivity towards a *rac*-epoxide, can be used to evaluate EH's enantiopreference in kinetic resolution [27]. Based on the measured *c* of *rac*-**6a**–**10a** at a range of 30–50% and ee_s of retained enantiomers, the *E* of *Gm*EH3 were calculated (Table 1). *Gm*EH3 showed low *E* of 7.4 and 5.2 towards *rac*-**6a** and **9a**, while the highest *E* of 55.6 towards *rac*-**7a**. The enantioselective reactions of 20 mM *rac*-**6a**–**10a** by 10 mg/mL wet cells were conducted until ee_s values of (*R*)-**6a**–**10a** reached over 99%. As a result, their $yield_s$ were from 17.1 to 43.5%. More interestingly, owing to the high *E* (55.6) and β_S (97.4%) of *Gm*EH3 for (*S*)-**7a**, the near-perfect kinetic resolution of *rac*-**7a** retained (*R*)-**7a** with 99.8% ee_s and 43.5% $yield_s$, and simultaneously generated (*S*)-**7b** with 88.9% ee_p and 49.5% $yield_p$. To the best of our knowledge, except for a *Tsukamurella paurometabola* EH (*Tp*EH1, E = 65) [28], *Gm*EH3 displayed the highest *E* value towards *rac*-**7a** among all known WT EHs, such as a *Rhodobacterales bacterium* EH (*R*EH, E = 38.4) (Table S4) [29].

3.5. Kinetic parameters of the purified GmEH3 for (S)- and (R)-5a (or 7a)

The kinetic parameters of purified *Gm*EH3 for enantiomeric **5a** or **7a** were shown in Table 2. The K_m^S (3.07 mM) and K_m^R (3.62 mM) for (*S*)- and (*R*)-**5a** were close to each other and the k_{cat}^S/K_m^S was only 1.64-fold higher than k_{cat}^R/K_m^R, suggesting that *Gm*EH3 had no obvious preference for (*S*)-**5a**, i.e., a very low *E* towards *rac*-**5a**. Together with its high and complementary regioselectivities (α_S = 89.4% and β_R = 90.6%) and high EH activity (22.4 U/g wc) (Table 1), it is suitable to produce enantiopure (*R*)-**5b** via the enantioconvergent hydrolysis of *rac*-**5a**. Contrarily, the K_m^S (3.61 mM) for (*S*)-**7a** was much lower than K_m^R (12.45 mM) for (*R*)-**7a**, indicating that *Gm*EH3 possessed stronger affinity with (*S*)-**7a** than (*R*)-**7a** [14]. The *E* value, derived from calculating the ratio of catalytic efficiency, $(k_{cat}^S/K_m^S)/(k_{cat}^R/K_m^R)$, was 57.3, which was very close to the result (E = 55.6) obtained via the hydrolysis of *rac*-**7a** using *E. coli/gmeh3*. The high *E* value and EH activity (35.1 U/g wc) enabled *Gm*EH3 to efficiently catalyze the kinetic resolution of *rac*-**7a**.

3.6. Gram-scale enantioconvergent production of (R)-5b by E. coli/gmeh3

The concentrations (10 and 20 mM) of *rac*-**5a** for the assays of *Gm*EH3 activity, *E* value and regioselectivity coefficient, were too low to realize the capacity of *Gm*EH3 for gram-scale production of (*R*)-**5b**. In view of this, the regioselective hydrolytic reactions of *rac*-**5a** at 50, 100, 150 and 200 mM, in four aliquots of 2 mL phosphate buffer systems were conducted, respectively, at 25 °C within 8.0 h by *E. coli/gmeh3* cells (Table S5). Until the concentration of *rac*-**5a** up to 150 mM, it was almost completely hydrolyzed (c > 99%) within 1.5 h, producing (*R*)-**5b** with over 90% ee_p and 95% $yield_p$. However, in the case of 200 mM *rac*-**5a**, its *c* value and $yield_p$ reached only 80.2% and 76.5%, even though the reaction was prolonged to 8.0 h, suggesting severe inhibitory and/or denaturation effects of substrate (*rac*-**5a**) or its corresponding 1,2-diol product on EH activity of *E. coli/gmeh3*. This phenomenon also existed in other stereoselective hydrolytic reactions of *rac*-epoxides by EHs, such as *Tp*EH1 and an EH from *Aspergillus niger* (*An*EH) [28,30]. Consequently, the MAC of *rac*-**5a** was confirmed as 150 mM.

Generally, using whole cells instead of crude cell extract or purified enzyme as the biocatalyst was because that the former was easily obtained and had higher stability and tolerance during the reaction process [31]. The hydrolytic process of 150 mM (18.0 g/L) *rac*-**5a** using *E. coli/gmeh3* cells in the 50 mL phosphate buffer system was shown in Fig. 5a. After incubation for 1.5 h, *rac*-**5a** was almost completely

Table 1
Substrate spectrum assay of *E. coli/gmeh3* wet cells towards *rac*-**1a**-**10a**.

Epoxide	Activity (U/g wet cell)	*E*	α_S (%)	β_R (%)	ee_s (%)	ee_p (%)	$Yield_s$ (%)	$Yield_p$ (%)
1a	28.2	1.7	90.4	97.5	–[a]	88.5 (*R*)[b]	–	93.8 (*R*)
2a	9.8	6.9	89.1	90.4	–	78.5 (*R*)	–	71.2 (*R*)
3a	4.2	8.2	93.4	88.9	–	82.1 (*R*)	–	68.1 (*R*)
4a	18.2	1.3	85.8	87.4	–	72.1 (*R*)	–	92.9 (*R*)
5a	**22.4**	**1.6**	**93.7**	**97.2**	–	**90.1 (*R*)**	–	**94.5** (*R*)
6a	2.6	7.4	5.8	94.5	99.6 (*R*)	26.5 (*S*)	23.6 (*R*)	–
7a	**35.1**	**55.6**	**4.7**	**97.4**	**99.8 (*R*)**	**88.9 (*S*)**	**43.5 (*R*)**	**49.5 (*S*)**
8a	25.6	15.6	3.7	95.2	99.1 (*R*)	58.2 (*S*)	33.5 (*R*)	–
9a	10.0	5.2	7.8	93.4	99.2 (*R*)	34.7 (*S*)	17.1 (*R*)	–
10a	28.8	12.4	7.7	91.9	99.4 (*R*)	43.2 (*S*)	30.5 (*R*)	–

[a] Not determine.
[b] Configuration.

hydrolyzed (Fig. S2a), generating (*R*)-**5b** with 90.2% ee_p and 95.4% $yield_p$. Its STY_p was calculated to be 16.3 g/L/h, which was the highest ever reported, was 32.6-fold higher than that (0.5 g/L/h) by *E. coli/pveh1*^{Y3Z2} [26]. As the hydrolysis of *rac*-**5a** was continued to 2.0 h, the $yield_p$ and ee_p of (*R*)-**5b** had no obvious improvement.

3.7. Gram-scale production of (*R*)-**7a** via the kinetic resolution of *rac*-**7a**

Analogously, the enantioselective hydrolytic reactions of *rac*-**7a** at concentrations of 100, 200, 300, 400, 500 and 600 mM were carried out, respectively, at 25 °C within 8.0 h by *E. coli/gmeh3* cells. As shown in Table S6, the MAC of *rac*-**7a** was confirmed to be 500 mM (at 2.5 h), was higher than all those of EHs previously reported, such as 80 mM of *R*EH and 400 mM of *Tp*EH1 [28,29]. As the concentration of *rac*-**7a** was elevated to 600 mM, its *c* and the ee_s of (*R*)-**7a** was merely 48.8% and 78.1% until 8.0 h. The scale-up kinetic resolution of 500 mM (75.1 g/L) *rac*-**7a** using *E. coli/gmeh3* whole cells was performed in the 30 mL phosphate buffer system, and monitored by chiral HPLC at the given intervals (Fig. 5b). When *rac*-**7a** was incubated for 2.5 h, (*S*)-**7a** was almost entirely hydrolyzed at the *c* of 57.5% (Fig. S2b), retaining (*R*)-**7a** with over 99% ee_s and 43.2% $yield_s$. The STY_s of (*R*)-**7a** reached 13.0 g/L/h, being 7.65-fold that by *Bm*EH-expressing *Bacillus megaterium* whole cells, while 0.43-fold that by *Tp*EH1-expressing *T. paurometabola* cells [28,32].

3.8. Elucidation on the high regio- and enantio-selectivities of GmEH3

The modeled 3-D structure of *Gm*EH3 was composed of an α/β and a cap domains (Fig. S3). And its SBP, harboring a cluster of amino acid residues such as a catalytic triad (Asp^{101}-His^{299}-Asp^{264}) and two proton donors (Tyr^{152} and Tyr^{234}), was located between the α/β and cap domains. These structural characteristics were similar with other α/β EHs, such as *Pv*EH3 and *An*EH [13,33]. The substrate affinity and catalytic efficiency of enzymes tightly lie on the frequencies of nucleophile- or electrophile-present near attack conformation, that is, several geometric conditions have to be met [34]. For docked EH–epoxide complex, the lengths of l_1 and l_2 as well as the d_α and d_β were regarded as crucial parameters for explaining the frequencies of these nucleophilic attacks. In present study, to elucidate the sources of high regiocomplementarity and enantioselectivity of *Gm*EH3 towards *rac*-**5a** and **7a**, the docked complexes of *Gm*EH3 with (*S*)- and (*R*)-**5a** (or **7a**) were conducted and optimized, respectively (Fig. 6). As expected, the simulated results were highly accordant with the experimental measurements, and also similar to the conclusions summarized by other teams [35–37]. In detail, the lengths of l_1 and l_2 in *Gm*EH3–(*S*)-**5a** or –(*R*)-**5a** were all less than 3.2 Å, which were the prerequisites for smooth ring-opening hydrolysis [38]. Furthermore, d_α of *Gm*EH3–(*S*)-**5a** (or d_β of *Gm*EH3–(*R*)-**5a**) was obviously shorter than d_β of *Gm*EH3–(*S*)-**5a** (or d_α of *Gm*EH3–(*R*)-**5a**), supporting the fact that C_α of (*S*)-**5a** and C_β of (*R*)-**5a** were mainly (with probabilities over 93% according to α_S and β_R values listed in Table 1) attacked by *Gm*EH3. Similarly, both the l_1 and l_2 of *Gm*EH3–(*S*)-**7a** were less than 3.2 Å, while, in the case of (*R*)-**7a**, they were more than 3.2 Å, indicating that *Gm*EH3 showed higher affinity for (*S*)-**7a** than (*R*)-**7a**. Because of the rapid hydrolytic rate of (*S*)-**7a** and

Table 2
Kinetic parameters of purified *Gm*EH3 for enantiomeric **5a** and **7a**.

Substrate	V_{max} (μmol/min/mg)	k_{cat} (s^{-1})	K_m (mM)	k_{cat}/K_m (mM^{-1} s^{-1})
(*S*)-**5a**	12.30 ± 0.66	7.68	3.07 ± 0.21	2.50
(*R*)-**5a**	8.80 ± 0.42	5.49	3.62 ± 0.19	1.52
(*S*)-**7a**	29.83 ± 1.12	18.62	3.61 ± 0.21	5.16
(*R*)-**7a**	1.77 ± 0.09	1.10	12.45 ± 0.64	0.09

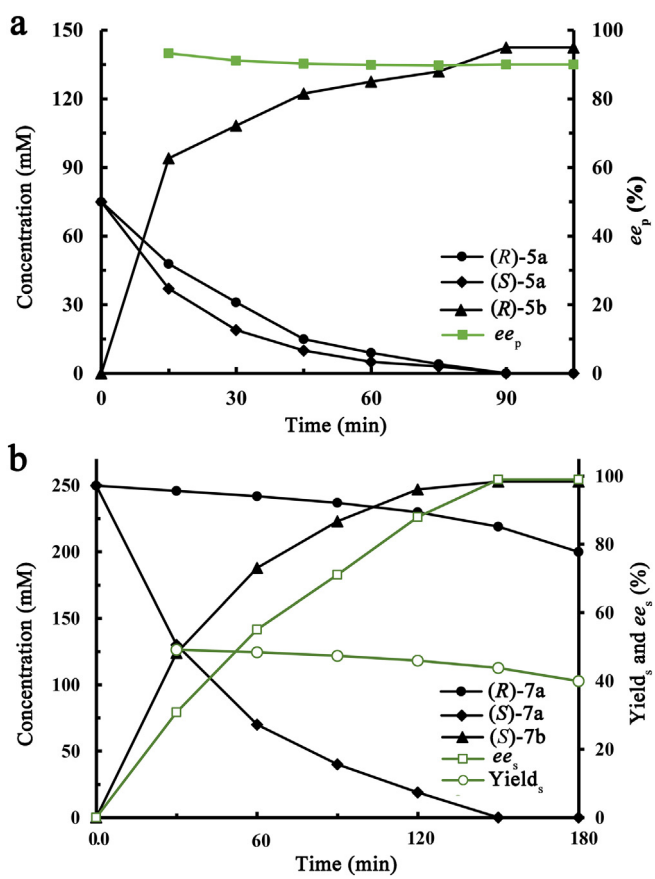

Fig. 5. The gram-scale enantioconvergence hydrolysis of *rac*-**5a** (a) and kinetic resolution of *rac*-**7a** (b) by *E coli/gemh3* whole cells.

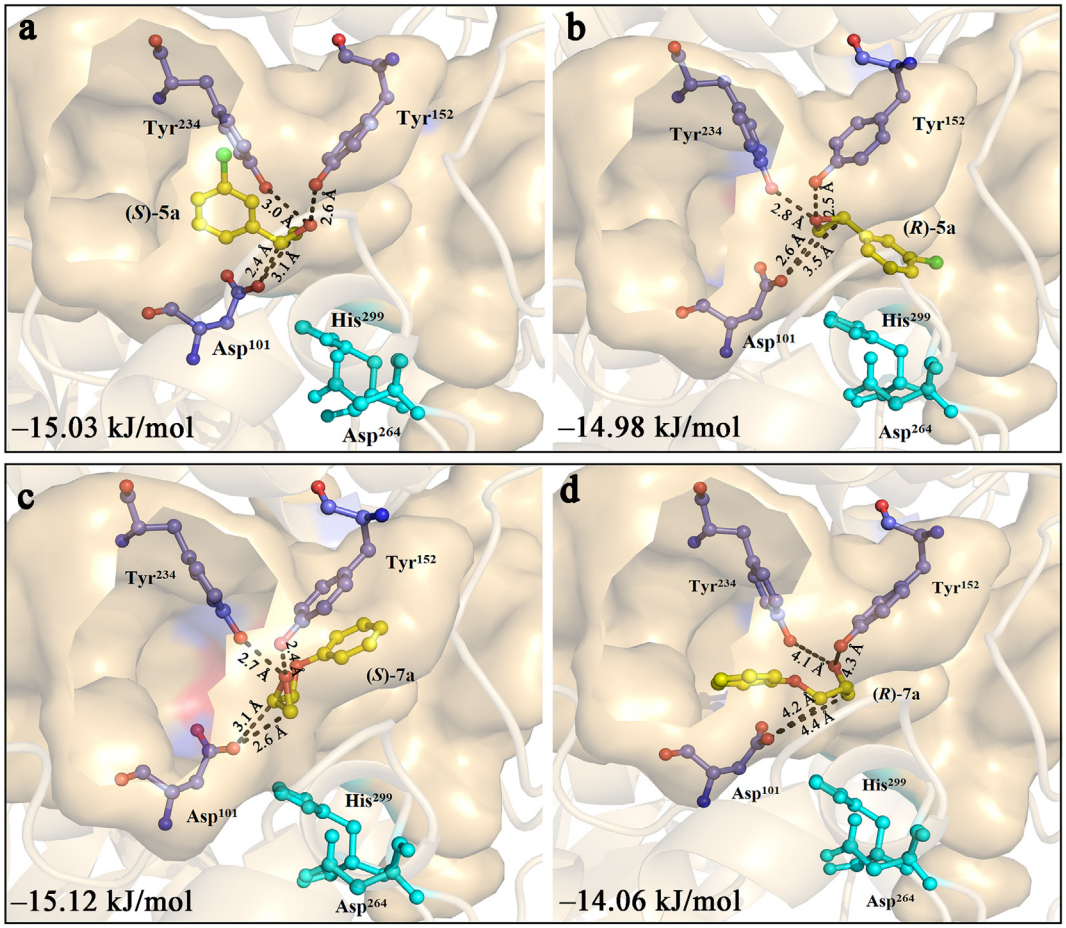

Fig. 6. MD simulations of (*S*)- and (*R*)-**5a** (or **7a**) with *Gm*EH3. The locally magnified 3-D conformations of *Gm*EH3-(*S*)-**5a** (a) or -(*S*)-**7a** (c) were compared with those of *Gm*EH3-(*R*)-**5a** (b) or -(*R*)-**7a** (d), respectively.

inert (*R*)-**7a** in the kinetic resolution of *rac*-**7a**, it is meaningful to individually take *Gm*EH3–(*S*)-**7a** into account. In *Gm*EH3–(*S*)-**7a**, the comparatively shorter d_{β} suggested that C_{β} of (*S*)-**7a** was mainly attacked, which conformed to the high enantioselectivity of *Gm*EH3 with preference for (*S*)-**7a**. Besides, these four EH–substrate complexes possessed $\Delta G_{binding}$ values ranging from −15.12 to −14.06 kJ/mol.

4. Conclusions

Based on the computer-aided analysis, a novel EH, *Gm*EH3 from *G. max* was excavated, then a *Gm*EH3-encoding gene, *gmeh3*, was successfully cloned, and heterologously expressed in *E. coli* Rosetta(DE3). The substrate spectrum assay indicated that *Gm*EH3 possessed the excellent regiocomplementarity for (*S*)- and (*R*)-**5a** and highest enantioselectivity towards *rac*-**7a**, among ten investigated *rac*-epoxides. Additionally, the gram-scale enantioconvergent hydrolysis of *rac*-**5a** and kinetic resolution of *rac*-**7a** at MAC were conducted using whole cells of *E. coli*/*gmeh3*, producing (*R*)-**5b** or (*R*)-**7a** with high enantiopurity and yield. All these superior catalytic performances make *Gm*EH3 an attractive biocatalyst for producing enantiopure epoxides and/or 1,2-doils. Moreover, the sources of high regiocomplementarity and enantioselectivity of *Gm*EH3 towards *rac*-**5a** and **7a** were explained by MD simulation.

Author statement

Min-chen Wu and Jun Zhao conceived and designed the experiments, also revised the manuscript; Chen Zhang and Chuang Li performed the experiments and wrote the draft; Xiu-xiu Zhu and You-yi Liu analyzed the data.

Declaration of competing interest

All of authors declare they have no commercial or financial conflict of interest.

Acknowledgement

This work was financially supported by the National Natural Science Foundation of China (No. 21676117), and the National First-Class Discipline Program of Food Science and Technology of China (JUFSTR20180101). We are grateful to Prof. Xian-zhang Wu for providing technical assistance.

Appendix A. Supplementary data

Supplementary data to this article can be found online at https://doi.org/10.1016/j.ijbiomac.2020.08.011.

References

[1] F.C. Huang, W. Schwab, Molecular characterization of *Nb*EH1 and *Nb*EH2, two epoxide hydrolases from *Nicotiana benthamiana*, Phytochemistry 90 (2013) 6–15.
[2] M. Widersten, A. Gurell, D. Lindberg, Structure-function relationships of epoxide hydrolases and their potential use in biocatalysis, Biochim. Biophys. Acta Gen. Subj. 1800 (2010) 316–326.
[3] M. Arand, A. Cronin, F. Oesch, S.L. Mowbray, T.A. Jones, The telltale structures of epoxide hydrolases, Drug Metab. Rev. 35 (2003) 365–383.

[4] M.E.S. Lind, F. Himo, Quantum chemical modeling of enantioconvergency in soluble epoxide hydrolase, ACS Catal. 6 (2016) 8145–8155.
[5] M. Kotik, A. Archelas, R. Wohlgemuth, Epoxide hydrolases and their application in organic synthesis, Curr. Org. Chem. 16 (2012) 451–482.
[6] M. Kotik, V. Štěpánek, M. Grulich, P. Kyslík, A. Archelas, Access to enantiopure aromatic epoxides and diols using epoxide hydrolases derived from total biofilter DNA, J. Mol. Catal. B Enzym. 65 (2010) 41–48.
[7] D. Hu, C.D. Tang, C. Li, T.T. Kan, X.L. Shi, L. Feng, M.C. Wu, Stereoselective hydrolysis of epoxides by re*Vr*EH3, a novel *Vigna radiata* epoxide hydrolase with high enantioselectivity or high and complementary regioselectivity, J. Agric. Food Chem. 65 (2017) 9861–9870.
[8] X. Jia, Z. Wang, Z. Li, Preparation of (*S*)-2-, 3-, and 4-chlorostyrene oxides with the epoxide hydrolase from *Sphingomonas* sp. HXN-200, Tetrahedron Asymmetry 19 (2008) 407–415.
[9] M. Wittman, J. Carboni, R. Attar, B. Balasubramanian, P. Balimane, P. Brassil, F. Beaulieu, C. Chang, W. Clarke, J. Dell, J. Eummer, D. Frennesson, M. Gottardis, A. Greer, S. Hansel, W. Hurlburt, B. Jacobson, S. Krishnananthan, F.Y. Lee, A. Li, T.A. Lin, P. Liu, C. Ouellet, X. Sang, M.G. Saulnier, K. Stoffan, Y. Sun, U. Velaparthi, H. Wong, Z. Yang, K. Zimmermann, M. Zoeckler, D. Vyas, Discovery of a (1H-Benzoimidazol-2-yl)-1H-pyridin-2-one (BMS-536924) inhibitor of insulin-like growth factor I receptor kinase with in vivo antitumor activity, J. Med. Chem. 48 (2005) 5639–5643.
[10] M. Kloosterman, V.H.M. Elferink, J. van Iersel, J.-H. Roskam, E.M. Meijer, L.A. Hulshof, R.A. Sheldon, Lipases in the preparation of β-blockers, Trends Biotechnol. 6 (1988) 251–256.
[11] S.I. Mkofsky, S. Melamed, J.S. Cohen, J.R. Slight, G. Spaeth, R.A. Lewis, L.Z. Gutman, C.Y. Eto, J.C. Lue, G.D. Novack, A comparison of the ocular hypotensive efficacy of once-daily and twice-daily Levobunolol treatment, Ophthalmology 96 (1989) 8–11.
[12] J.S. Prasad, T. Vu, M.J. Totleben, G.A. Crispino, D.J. Kacsur, S. Swaminathan, J.E. Thornton, A. Fritz, A.K. Singh, Development of Jacobsen asymmetric epoxidation and Sharpless asymmetric dihydroxylation methods for the large-scale preparation of a chiral dihydrobenzofuran epoxide, Org. Process. Res. Dev. 7 (2003) 821–827.
[13] C. Zhang, Y.Y. Liu, C. Li, Y.H. Xu, Y.J. Su, J.F. Li, J. Zhao, M.C. Wu, Significant improvement in catalytic activity and enantioselectivity of a *Phaseolus vulgaris* epoxide hydrolase, *Pv*EH3, towards *ortho*-cresyl glycidyl ether based on the semi-rational design, Sci. Rep. 10 (2020) 1680.
[14] B.C. Hu, D. Hu, C. Li, X.F. Xu, Z. Wen, M.C. Wu, Near-perfect kinetic resolution of racemic *p*-chlorostyrene oxide by *Sl*EH1, a novel epoxide hydrolase from *Solanum lycopersicum* with extremely high enantioselectivity, Int. J. Biol. Macromol. 147 (2020) 1213–1220.
[15] D. Hu, C.D. Tang, B. Yang, J.C. Liu, T. Yu, C. Deng, M.C. Wu, Expression of a novel epoxide hydrolase of *Aspergillus usamii* E001 in *Escherichia coli* and its performance in resolution of racemic styrene oxide, J. Ind. Microbiol. Biotechnol. 42 (2015) 671–680.
[16] C. Li, T.T. Kan, D. Hu, T.T. Wang, Y.J. Su, C. Zhang, J.Q. Cheng, M.C. Wu, Improving the activity and enantioselectivity of *Pv*EH1, a *Phaseolus vulgaris* epoxide hydrolase, for *o*-methylphenyl glycidyl ether by multiple site-directed mutagenesis on the basis of rational design, Mol. Catal. 476 (2019) 110517.
[17] B.C. Hu, C. Li, R. Wang, X.C. Zong, J.P. Li, J.F. Li, M.C. Wu, Improvement in the activity and enantioconvergency of *Pv*EH3, an epoxide hydrolase from *Phaseolus vulgaris*, for *p*-chlorostyrene oxide by site-saturation mutagenesis, Catal. Commun. 117 (2018) 9–13.
[18] C. Li, D. Hu, X.C. Zong, C. Deng, L. Feng, M.C. Wu, J.F. Li, Asymmetric hydrolysis of styrene oxide by *Pv*EH2, a novel *Phaseolus vulgaris* epoxide hydrolase with extremely high enantioselectivity and regioselectivity, Catal. Commun. 102 (2017) 57–61.
[19] S. Barth, M. Fischer, R.D. Schmid, J. Pleiss, Sequence and structure of epoxide hydrolases: a systematic analysis, Proteins 55 (2004) 846–855.
[20] G.A. Gomez, C. Morisseau, B.D. Hammock, D.W. Christianson, Structure of human epoxide hydrolase reveals mechanistic inferences on bifunctional catalysis in epoxide and phosphate ester hydrolysis, Biochemistry 43 (2004) 4716–4723.
[21] M. Arahira, V.H. Nong, K. Udaka, C. Fukazawa, Purification, molecular cloning and ethylene-inducible expression of a soluble-type epoxide hydrolase from soybean (*Glycine max* [L.] Merr.), Eur. J. Biochem. 267 (2000) 2649–2657.
[22] Q.Q. Zhu, W.H. He, X.D. Kong, L.Q. Fan, J. Zhao, S.X. Li, J.H. Xu, Heterologous overexpression of *Vigna radiata* epoxide hydrolase in *Escherichia coli* and its catalytic performance in enantioconvergent hydrolysis of *p*-nitrostyrene oxide into (*R*)-*p*-nitrophenyl glycol, Appl. Microbiol. Biotechnol. 98 (2014) 207–218.
[23] H.H. Ye, D. Hu, X.L. Shi, M.C. Wu, C. Deng, J.F. Li, Directed modification of a novel epoxide hydrolase from *Phaseolus vulgaris* to improve its enantioconvergence towards styrene epoxides, Catal. Commun. 87 (2016) 32–35.
[24] A. Stapleton, J.K. Beetham, F. Pinot, J.E. Garbarino, D.R. Rockhold, M. Friedman, B.D. Hammock, W.R. Belknap, Cloning and expression of soluble epoxide hydrolase from potato, Plant J. 6 (1994) 251–258.
[25] M.I. Monterde, M. Lombard, A. Archelas, A. Cronin, R. Furstoss, Enzymatic transformations. Part 58: enantioconvergent biohydrolysis of styrene oxide derivatives catalysed by the *Solanum tuberosum* epoxide hydrolase, Tetrahedron Asymmetry 15 (2004) 2801–2805.
[26] X.C. Zong, C. Li, Y.H. Xu, D. Hu, B.C. Hu, J. Zang, M.C. Wu, Substantially improving the enantioconvergence of *Pv*EH1, a *Phaseolus vulgaris* epoxide hydrolase, towards *m*-chlorostyrene oxide by laboratory evolution, Microb. Cell Factories 18 (2019) 1–8.
[27] J.L.L. Rakels, A.J.J. Straathof, J.J. Heijnen, A simple method to determine the enantiomeric ratio in enantioselective biocatalysis, Enzym. Microb. Technol. 15 (1993) 1051–1056.
[28] K. Wu, H. Wang, H. Sun, D. Wei, Efficient kinetic resolution of phenyl glycidyl ether by a novel epoxide hydrolase from *Tsukamurella paurometabola*, Appl. Microbiol. Biotechnol. 99 (2015) 9511–9521.
[29] J.H. Woo, J.H. Kang, Y.O. Hwang, J.C. Cho, S.J. Kim, S.G. Kang, Biocatalytic resolution of glycidyl phenyl ether using a novel epoxide hydrolase from a marine bacterium, *Rhodobacterales bacterium* HTCC2654, J. Biosci. Bioeng. 109 (2010) 539–544.
[30] H.X. Jin, Z.C. Hu, Y.G. Zheng, Enantioselective hydrolysis of epichlorohydrin using whole *Aspergillus niger* ZJB-09173 cells in organic solvents, J. Biosci. 37 (2012) 695–702.
[31] E.Y. Lee, M.L. Shuler, Molecular engineering of epoxide hydrolase and its application to asymmetric and enantioconvergent hydrolysis, Biotechnol. Bioeng. 98 (2007) 318–327.
[32] J. Zhao, Y.Y. Chu, A.T. Li, X. Ju, X.D. Kong, J. Pan, Y. Tang, J.H. Xu, An unusual (*R*)-selective epoxide hydrolase with high activity for facile preparation of enantiopure glycidyl ethers, Adv. Synth. Catal. 353 (2011) 1510–1518.
[33] J. Zou, B.M. Hallberg, T. Bergfors, F. Oesch, M. Arand, S.L. Mowbray, T.A. Jones, Structure of *Aspergillus niger* epoxide hydrolase at 1.8 Å resolution: implications for the structure and function of the mammalian microsomal class of epoxide hydrolases, Structure 8 (2000) 111–122.
[34] T.C. Bruice, A view at the millennium: the efficiency of enzymatic catalysis, Acc. Chem. Res. 35 (2002) 139–148.
[35] C. Li, B.C. Hu, Z. Wen, D. Hu, Y.Y. Liu, Q. Chu, M.C. Wu, Greatly enhancing the enantioselectivity of *Pv*EH2, a *Phaseolus vulgaris* epoxide hydrolase, towards racemic 1,2-epoxyhexane via replacing its partial cap-loop, Int. J. Biol. Macromol. 156 (2020) 225–232.
[36] Z. Liu, L. Zhang, F. Cheng, L. Ruan, Z. Hu, Y. Zheng, Y. Shen, Characterization of a newly synthesized epoxide hydrolase and its application in racemic resolution of (*R*,*S*)-epichlorohydrin, Catal. Commun. 16 (2011) 133–139.
[37] F. Xue, Z. Liu, N. Wan, H. Zhu, Y. Zheng, Engineering the epoxide hydrolase from *Agromyces mediolanus* for enhanced enantioselectivity and activity in the kinetic resolution of racemic epichlorohydrin, RSC Adv. (2015) 31525–31532.
[38] M.T. Reetz, M. Bocola, L.W. Wang, J. Sanchis, A. Cronin, M. Arand, J.Y. Zou, A. Archelas, A.L. Bottalla, A. Naworyta, S.L. Mowbray, Directed evolution of an enantioselective epoxide hydrolase: uncovering the source of enantioselectivity at each evolutionary stage, J. Am. Chem. Soc. 131 (2009) 7334–7343.